Supplemental Material for "Trion formation and ordering in the attractive SU(3) Fermi-Hubbard model"

Jonathan Stepp,[1,*] Eduardo Ibarra-García-Padilla,[2] Richard T. Scalettar,[3] and Kaden R. A. Hazzard[1,4]

[1] *Department of Physics and Astronomy, Rice University, Houston, Texas 77005, USA*
[2] *Department of Physics, Harvey Mudd College, 301 Platt Blvd, Claremont, CA 91711, USA*
[3] *Department of Physics, University of California, Davis, California 95616, USA*
[4] *Smalley-Curl Institute, Houston, Texas 77005, USA*

(Dated: May 6, 2026)

I. DQMC METHOD

We can write the Hamiltonian for the attractive SU(N) Fermi-Hubbard model (FHM) as $H = Q + V$, where

$$Q = -t \sum_{\sigma,\langle i,j\rangle} \left[c^\dagger_{i\sigma} c_{j\sigma} + \text{h.c.}\right] - \mu \sum_{\sigma,i} n_{i\sigma}, \tag{S1}$$

$$V = -\frac{U}{2} \sum_i \left(\sum_\sigma n_{i\sigma} - \frac{N}{2}\right)^2. \tag{S2}$$

Here, i is the site index and σ is the molecular spin index. Then, the Determinant Quantum Monte Carlo (DQMC) we have developed for the attractive SU(N) FHM works by first Trotterizing the partition function

$$\mathcal{Z} = \text{Tr}\, e^{-\beta H} = \lim_{\Delta\tau\to 0} \left(e^{-\Delta\tau Q} e^{-\Delta\tau V}\right)^M, \tag{S3}$$

where $\beta = \frac{1}{T}$, T is the temperature (we set Boltzmann's constant $k_B = 1$ throughout), and $M \equiv \beta/\Delta\tau$ is the number of Trotter steps. We estimate the error caused by this Trotterization process and compare it to other sources of uncertainty in Section VI.

To handle the interaction term, V, we employ the Hubbard-Stratonovich transformation

$$\begin{aligned} e^{-\Delta\tau V} &= \prod_i e^{\Delta\tau \frac{U}{2} \sum_i \left(n_{i\sigma} - \frac{N}{2}\right)^2} \\ &= \prod_i \left(\frac{1}{\sqrt{2\pi}} \int_{-\infty}^{\infty} e^{-\frac{1}{2}x_i^2 - x_i\sqrt{\Delta\tau U}\left(\sum_\sigma n_{i\sigma} - \frac{N}{2}\right)} \mathrm{d}x_i\right), \end{aligned} \tag{S4}$$

which decomposes the interaction term into a non-interacting term at the cost of introducing a classical field x_i for each lattice site i. If we apply this Hubbard-Stratonovich transformation to each $e^{-\Delta\tau V}$ term in Eq. (S3), we obtain

$$\mathcal{Z} = \left(\frac{1}{\sqrt{2\pi}}\right)^{ML^2} \int \prod_{\ell,i} \mathrm{d}x_{i,\ell}\, \text{Tr}\left[\prod_{\ell=1}^{M} e^{-\Delta\tau Q} e^{-\Delta\tau \tilde{V}_\ell}\right], \tag{S5}$$

where ℓ goes from 1 to M, $\tilde{V}_\ell = \sum_i -\frac{1}{2}x_{i\ell}^2 - x_{i\ell}\sqrt{\Delta\tau U}\left(\Sigma_\sigma n_{i\sigma} - \frac{N}{2}\right)$, and the classical fields $x_{i\ell}$ have gained an index to specify both their lattice site index, i, and imaginary time step index, ℓ. Since Q and each of the $\tilde{V}_\ell$'s are quadratic in fermion creation/annihilation operators, we can treat the integrand as a non-interacting system. If we calculate analytic results about this non-interacting system and then use a Monte-Carlo process to integrate over the $x_{i\ell}$ fields, we obtain results about the attractive SU(N) FHM. As shown in Ref. [1], this results in

$$\begin{aligned} \mathcal{Z} &= \left(\frac{1}{\sqrt{2\pi}}\right)^{ML^2} \int \prod_{\ell,i} \mathrm{d}x_{i,\ell} \det M(\{x_{i\ell}\}) e^{-S_B(\{x_{i\ell}\})} \\ &= \left(\frac{1}{\sqrt{2\pi}}\right)^{ML^2} \int \prod_{\ell,i} \mathrm{d}x_{i,\ell} \left[\det M^\sigma(\{x_{i\ell}\})\right]^N e^{-S_B(\{x_{i\ell}\})}, \end{aligned} \tag{S6}$$

where $M(\{x_{i\ell}\})$ is a $NL^2 \times NL^2$ matrix and S_B is a leftover bosonic action. Since there are no molecule spin state-changing interactions, $M(\{x_{i\ell}\})$ is block diagonal in the molecular spin states, and each block is identical due to the SU(N) symmetry. Therefore, we can simplify the expression by defining $M^\sigma(\{x_{i\ell}\})$ as the $L^2 \times L^2$ matrix that makes up each block. Our notation emphasizes that each of these quantities depends on a specific configuration of the Hubbard-Stratonovich fields, $\{x_{i\ell}\}$.

During the Monte Carlo process, proposed changes are accepted based on the ratio between integrands in Eq. (S6). So the probability of accepting a change $\{x_{i\ell}\} \to \{x'_{i\ell}\}$ is given by

$$p\left(\{x_{i\ell}\} \to \{x'_{i\ell}\}\right) = \frac{\left[\det M^\sigma(\{x'_{i\ell}\})\right]^N}{\left[\det M^\sigma(\{x_{i\ell}\})\right]^N} e^{-\Delta S_B}, \tag{S7}$$

where $\Delta S_B = S_B(\{x_{i\ell}\}) - S_B(\{x'_{i\ell}\})$. Our DQMC implementation typically proposes changes which shift individual $x_{i\ell}$ variables by some amount one at a time. To improve convergence rates and avoid local minima, we also perform occasional "global moves" which propose changing every $x_{i\ell}$ for a given i at once.

While this looks like a straightforward application of Monte-Carlo integration, the matrix $M^\sigma(\{x_{i\ell}\})$ is not necessarily positive-definite for every choice of $\{x_{i\ell}\}$, which means $p\left(\{x_{i\ell}\} \to \{x'_{i\ell}\}\right)$ is not always positive. When this happens, $|p(\{x_{i\ell}\} \to \{x'_{i\ell}\})|$ can be used as the

* jds28@rice.edu

acceptance probability, and the standard DQMC measurements can still be performed. However, if the positive and negative sign regions of configuration space have comparable weight, the number of DQMC sweeps needed to resolve observables to a given error grows exponentially with decreasing error.

This exponential increase in required computational resources is the so-called "fermion sign problem" [2–4]. Note that if N is even, $[\det M^\sigma(\{x_{i\ell}\})]^N > 0$ for any field configuration so our DQMC implementation is sign problem free. Here, since $N = 3$, a sign problem can occur. By defining

$$\mathcal{S} = \begin{cases} 1 & \text{if} \quad [\det M^\sigma(\{x_{i\ell}\})]^N \geq 0 \\ -1 & \text{if} \quad [\det M^\sigma(\{x_{i\ell}\})]^N < 0 \end{cases} \tag{S8}$$

the measurement $\langle \mathcal{S} \rangle$ (called the sign), can be used to diagnose the severity of the sign problem. In a sign-problem free model, $\langle S \rangle = 1$ while in a model with a sign problem, $\langle S \rangle \to 0$ as $T \to 0$ or $L \to \infty$.

Lattice	T/t	U/t	μ/t	$\langle \mathcal{S} \rangle$
14×14	1/3	7.25	0	0.9899 ± 0.0101
14×14	1/3	7.75	0	0.9872 ± 0.0096
14×14	1/3	8.5	0	0.9295 ± 0.0705
14×14	1/3	8.75	0	0.8330 ± 0.1148

TABLE S1. The average sign, $\langle \mathcal{S} \rangle$, for all data points where $\langle S \rangle < 0.99$.

The largest source of numerical error for the calculations in this paper is generally finite-size errors (discussed in Supplemental Sec. V), not the sign problem. A few intermittent data points exhibited the beginning of a sign problem, but we did not observe the exponential scaling which would make calculations infeasible. In Table S1, we present the data points exhibiting the most severe sign problem out of all of our data. Outside of the points in Table S1, $\langle \mathcal{S} \rangle > 0.99$ for all data points.

The temperatures considered in this work were cold enough to observe the CDW phase and the trend $\chi \to 0$ in the bound trion regime. It is unclear if the sign problem would be an important limiting factor if we pushed to colder temperatures to attempt to observe the onset of CSF order.

II. COMPRESSIBILITY APPROXIMATIONS

This section develops approximations to understand the small- and large-U limits of the compressibility.

A. Weakly-interacting mean field

We use a Hartree approximation to treat the attractive SU(3) FHM in the weakly interacting limit ($U \ll t, \mu$). First, we re-write our Hamiltonian in a more convenient form:

$$H = \sum_\sigma \Bigg[-t \sum_{\langle i,j \rangle} c^\dagger_{i\sigma} c_{j\sigma} + \text{ h.c.} \\ - \sum_i \left((\mu - U)\, n_{i\sigma} + \frac{U}{2} \sum_{\tau \neq \sigma} n_{i\sigma} n_{i\tau} \right) \Bigg]. \tag{S9}$$

We can then obtain our mean field Hamiltonian by expanding the density operators around their average values and dropping second-order terms. So,

$$H_{\text{MF}} = \sum_\sigma \Bigg[-t \sum_{\langle i,j \rangle} c^\dagger_{i\sigma} c_{j\sigma} + \text{ h.c.} \; - \sum_i (\mu - U) n_{i\sigma} \\ - \frac{U}{2} \sum_{\tau \neq \sigma} \langle n_{i\sigma} \rangle n_{i\tau} + \langle n_{i\tau} \rangle n_{i\sigma} - \langle n_{i\sigma} \rangle \langle n_{i\tau} \rangle \Bigg]. \tag{S10}$$

Then, setting $\langle n_{i\sigma} \rangle = \bar{n}$ for each i and σ, we obtain the non-interacting mean field Hamiltonian

$$\begin{aligned} H_{\text{MF}} &= \sum_{\mathbf{k},\sigma} (\varepsilon_{\mathbf{k}} - \mu - U(2\bar{n} - 1)) n_{\mathbf{k},\sigma} \\ &= \sum_{\mathbf{k},\sigma} (\varepsilon_{\mathbf{k}} - z) n_{\mathbf{k},\sigma}, \end{aligned} \tag{S11}$$

where $\mathbf{k} = (2\pi n_x/L, 2\pi n_y/L)$ for integers $n_x, n_y \in [0, L)$, $\varepsilon_{\mathbf{k}} = -2t(\cos(k_x) + \cos(k_y))$, and $z = \mu - U(2\bar{n} - 1)$.

The Hartree approximation is computed by self-consistently solving

$$\bar{n} = \frac{1}{L^2} \sum_{\mathbf{k}} \frac{1}{1 + \exp\left[\beta(\varepsilon_{\mathbf{k}} - z)\right]} \tag{S12}$$

for $\bar{n}$. Then, the single-component isothermal compressibility is

$$\kappa = \frac{\kappa_0(\beta, t, z, L)}{1 - 2U\bar{n}^2 \kappa_0(\beta, t, z, L)}, \tag{S13}$$

where

$$\kappa_0(\beta, t, z, L) = \frac{\beta}{\bar{n}^2 L^2} \sum_{\mathbf{k}} \frac{1}{2 + 2\cosh(\beta(\varepsilon_{\mathbf{k}} - z))} \tag{S14}$$

is the isothermal compressibility for a non-interacting single fermion-species on an $L \times L$ square lattice.

B. Classical ideal gas of trions

Starting from

$$\kappa = \frac{1}{n^2} \left(\frac{\partial n}{\partial \mu} \right)_{T,L}, \tag{S15}$$

we can use the Gibbs-Duhem relation to write that

$$\kappa = -\frac{1}{V}\left(\frac{\partial V}{\partial p}\right)_{T,\mu}. \tag{S16}$$

Then, using the equation of state for a classical ideal gas,

$$pV = NT, \tag{S17}$$

we can compute

$$\kappa = \frac{1}{nT}, \tag{S18}$$

where $n = \frac{N}{V}$ is the density of particles we are considering.

For our classical ideal gas approximation, we assume we are deep in the trion regime, so $n_{\text{tri}} = \frac{1}{3}\sum_\sigma n_\sigma$. For a useful comparison with our DQMC data, we calculate our κ by using the density reported by our DQMC and Eq. (S18).

C. Atomic limit

For the atomic limit calculation, we solve the one site problem, which is a valid approximation in the $U \gg t$ limit. For a single site, we have that

$$\mathcal{Z} = \sum_{k=0}^{3} \binom{3}{k} e^{\beta\mu k + \frac{\beta U}{2}(\frac{3}{2}-k)^2}, \tag{S19}$$

and

$$\langle n_\sigma \rangle = \frac{1}{\mathcal{Z}} \sum_{k=1}^{3} \binom{2}{k-1} e^{\beta\mu k + \frac{\beta U}{2}(\frac{3}{2}-k)^2}. \tag{S20}$$

We also have that

$$\left(\frac{\partial \langle n_\sigma \rangle}{\partial \mu}\right)_T = \frac{\beta}{\mathcal{Z}} \sum_{k=1}^{3} k \binom{2}{k-1} e^{\beta\mu k + \frac{\beta U}{2}(\frac{3}{2}-k)^2}, \tag{S21}$$

which allows us to calculate κ. Since we apply this approximation in the limit where $|\beta U| \gg |\beta\mu|$, we can obtain a useful limit by evaluating only $k = 0, 3$ terms in each of these sums. This gives us

$$\kappa = 3\beta(1 + e^{-3\beta\mu}), \tag{S22}$$

which, for $\mu < 0$, increases exponentially with β.

III. THE INVARIANT CORRELATION RATIO

As one way to pinpoint the finite-temperature phase transitions into the CDW phase, we introduce the invariant correlation ratio,

$$R_{\text{cdw}} = 1 - \frac{S_{\text{cdw}}(\mathbf{Q}+\delta\mathbf{q})}{S_{\text{cdw}}(\mathbf{Q})}, \tag{S23}$$

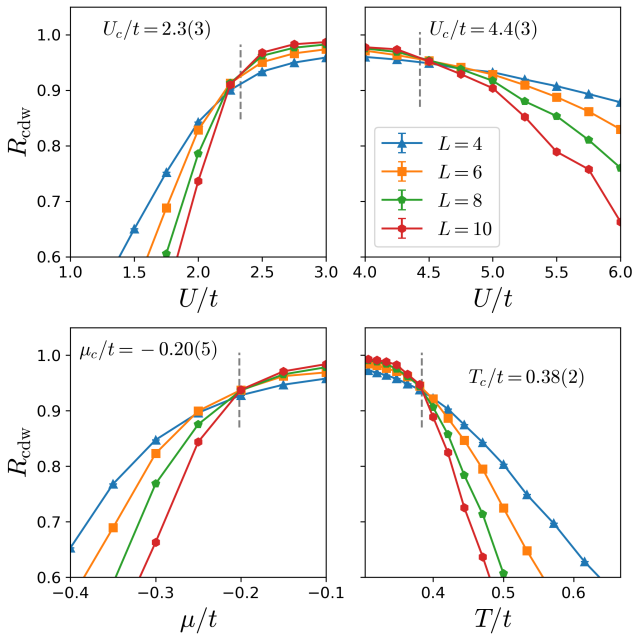

FIG. S1. The invariant correlation ratio for different lattice sizes. The crossings in the U, μ, and T directions provide evidence of the CDW phase transition and estimate the phase boundary as a function of each variable. The $L = 8$ to $L = 10$ crossings are all indicated by dashed gray lines with the critical values listed in each plot. Plots are all at $\mu = 0, U = 3.5t, T = t/3$ unless otherwise specified by the axis label.

where $\mathbf{Q}+\delta\mathbf{q}$ is a neighboring reciprocal lattice vector to $\mathbf{Q} = (\pi, \pi)$. By finite-size scaling arguments, this quantity will reach 1 in an ordered state, 0 in a disordered state and achieves a lattice-size independent value at a critical point [5, 6]. This allows us to identify the transition point near the resolution of our data points without introducing an artificial cutoff value.

As shown in Fig. S1 crossing behavior occurs along the boundary of the CDW phase in the U, μ and T directions which gives further evidence of a well-defined finite-temperature ordered phase. Here, the uncertainty is reported using the distance between successive data points.

IV. NUMERICAL DIFFERENTIATION

For the calculation of χ and κ, we needed to take a derivative with respect to μ. For both of these quantities, we used a simple first-order formula using only one additional DQMC run,

$$\frac{\partial \mathcal{O}}{\partial \mu} \approx \frac{\mathcal{O}(\mu) - \mathcal{O}(\mu - \Delta\mu)}{\Delta\mu}, \tag{S24}$$

where $\mathcal{O}$ is the expectation value we are differentiating and $\Delta\mu = 0.05t$.

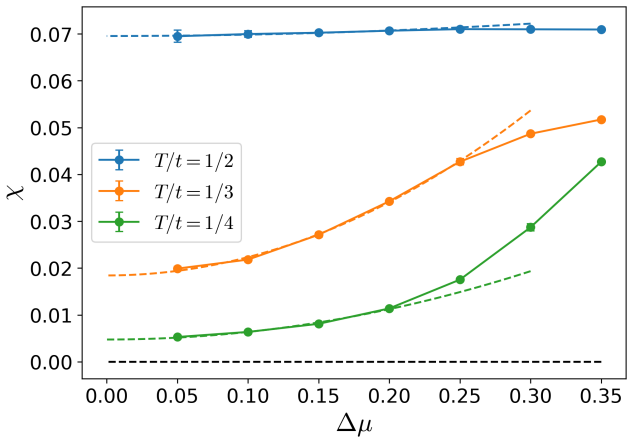

FIG. S2. The difference susceptibility χ, calculated as in Eq. (S24) with different $\Delta\mu$ for various temperatures at $\mu = 0$, $U = 3.5t$, and $L = 10$. The dashed lines indicate quadratic fits to the first 4 data points

In Fig. S2, we show how χ depends on the choice of $\Delta\mu$ and calculate an extrapolation for $\Delta\mu \to 0$ at various temperatures using a form

$$\chi = a + b(\Delta\mu)^2. \tag{S25}$$

The difference between the $\Delta\mu = 0.05t$ value and the $\Delta\mu \to 0$ extrapolated value is shown in Table S3.

For heat capacity data, we chose points which were equally spaced in $\beta = 1/T$. So, we differentiated using the chain rule and a second-order derivative formula,

$$\frac{\partial \mathcal{O}}{\partial T} \approx \frac{1}{T^2} \frac{\mathcal{O}(\beta - \Delta\beta) - \mathcal{O}(\beta + \Delta\beta)}{2\Delta\beta}, \tag{S26}$$

where $\mathcal{O}$ is the T-dependent quantity we are differentiating and where $t\Delta\beta = 0.125$.

In both cases, the statistical uncertainty reported for these quantities was calculated via error propagation of Eq. (S24) and Eq. (S26).

V. FINITE-SIZE EXTRAPOLATION

Since the DQMC method calculates properties on a finite-size lattice and we are interested in phase transitions — which necessarily only occur in the infinite-size limit — it is necessary to extrapolate the finite-size cases to the infinite-size case.

We begin with a discussion of the finite-size extrapolation for the difference susceptibility, χ. Since χ is the derivative of a difference of densities, we expect χ to approach a constant as $L \to \infty$. The simplest *ansatz* is

$$\chi(L) = A_\chi + \frac{B_\chi}{L}, \tag{S27}$$

where A_χ and B_χ parametrize the fit. Indeed, as shown in Fig. S3 this form is a good fit. As U/t increases, $B_\chi \to 0$, so while χ is affected by finite-size effects at low U/t, the qualitative picture of a sharpening crossover is not affected. This finite-size analysis also provides support for our choice to report only the $L = 10$ data in the main text.

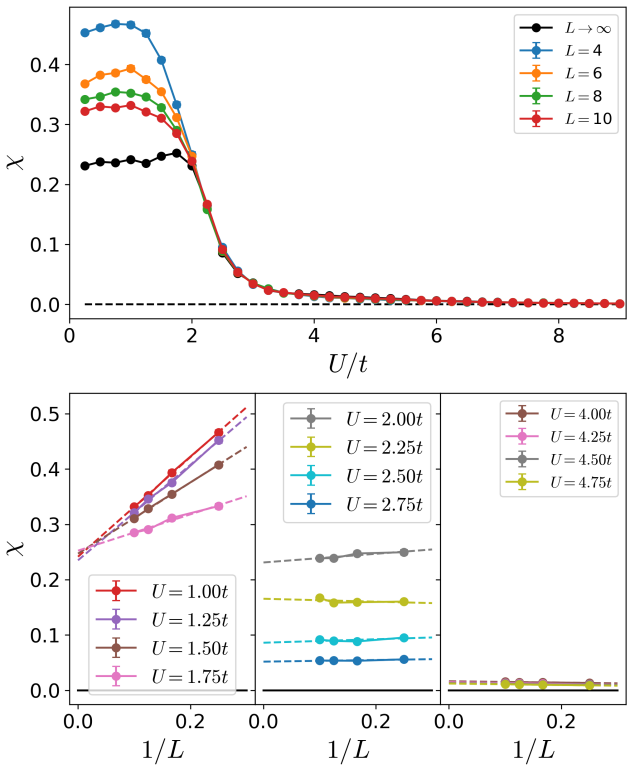

FIG. S3. Top: The difference susceptibility, χ at $T = t/3$ and $\mu = 0$ for different lattice sizes. The finite-size extrapolation (using Eq. (S27)) is shown in black. Bottom: The difference susceptibility χ as a function of $1/L$. The dashed lines show the fits for various values of U/t.

While the finite-size extrapolation was straightforward for χ, the CDW order parameter, S_{cdw}/L^2, presents a more complicated case. Near the CDW transition, S_{cdw}/L^2 has a clear system-size dependence, so to extrapolate to the infinite-size case, we fit to the functional form

$$\frac{1}{L}\sqrt{S_{\text{cdw}}(L)} = A + \frac{B}{L} + \frac{C}{L^2}. \tag{S28}$$

This form has been used to analyze a corresponding CDW QPT for attractive, SU(3) fermions on a two-dimensional honeycomb lattice [7].

On the other hand the functional form,

$$\frac{1}{L^2} S_{\text{cdw}}(L) = D + \frac{E}{L^2}, \tag{S29}$$

has also been used for a CDW transition on a honeycomb lattice and is motivated by spin wave theory [8, 9].

We compare these two functional forms in Fig. S4. The finite-size extrapolations are all based on the data

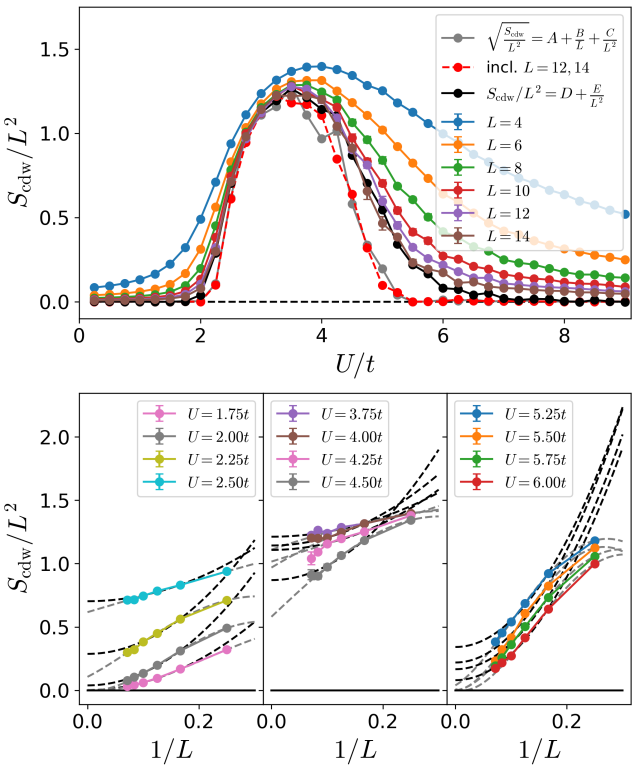

FIG. S4. Top: The CDW structure factor at $T = t/3$ and $\mu = 0$ for different lattice sizes. The finite-size extrapolations of the $L = 4, 6, 8, 10$ points using Eq. (S28) and Eq. (S29) are shown in gray and black respectively. The red dashed line shows a finite-size extrapolation using Eq. (S28) which includes the $L = 12, 14$ data points for comparison

Bottom: The CDW structure factor as a function of $1/L$ along with the fits for various ranges of U/t.

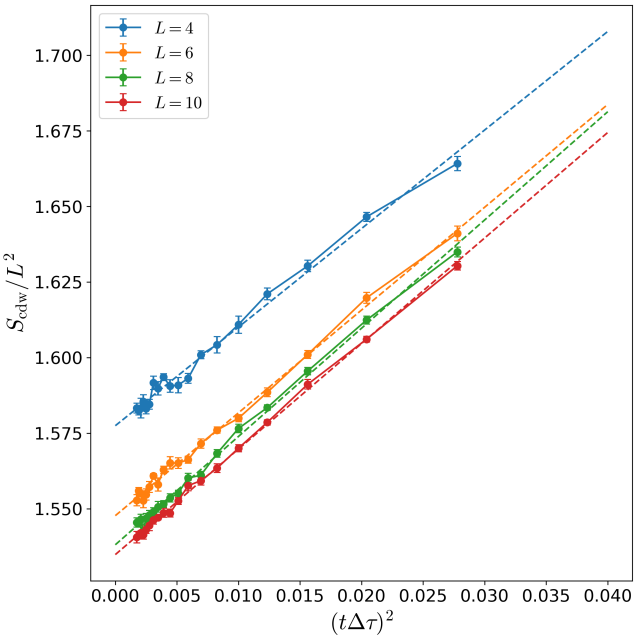

FIG. S5. The CDW structure factor at $U = 3.5t, \mu = 0, T = t/4$ as a function of $(t\Delta\tau)^2$. The dashed lines show a linear fit in $(t\Delta\tau)^2$.

up to size $L = 10$, where we have excluded the $L = 4$ data points from the extrapolations based on the form in Eq. (S29). For a consistency check, we have included data points for $L = 12, 14$ for $T = t/3$ and displayed those data points on top of the finite-size extrapolations based on the $L \leq 10$ data. While the form in Eq. (S29) seems smoother and closer to the $L = 10$ data point, we can see that the form in Eq. (S28) resolves sharp behavior at both low- and high-U/t. The form in Eq. (S28) also gives a high-U/t transition out of the CDW phase which agrees more closely with the U_c/t predicted by the invariant ratio analysis. We also note that the $L = 12$ and $L = 14$ data points are reasonably consistent with the Eq. (S28) fit, even in the region around $U \simeq 5.5t$ which has the most prominent finite-size effects. Additionally, including the $L = 12, 14$ data points only causes small changes to the finite-size extrapolation with the form in Eq. (S28). Thus, we used the functional form in Eq. (S28) and the $L = 4, 6, 8, 10$ data for the curve shown in Fig. 2 of the main text. The error bars in Fig. 2 are determined by the difference between the $L = 10$ data and the $L \to \infty$ extrapolation.

VI. SOURCES OF UNCERTAINTY

The DQMC algorithm depends on a Trotter decomposition of the Hamiltonian as shown in Eq. (S3). In Fig. S5, we compute the CDW structure factor for a range of $t\Delta\tau$ at a specific point in the CDW phase using the same number of DQMC sweeps as in other results. The smallest value of $t\Delta\tau$ in this chart is $t\Delta\tau = 1/24$ and we can see that our results are well-converged at this value. It is also clear on this graph that we are able to resolve finite-size effects and observe that the Trotter error is of a similar magnitude to the DQMC statistical error. Additionally, we fit this data to a quadratic function in $t\Delta\tau$ and compute the relative error between our measured data point and the $t\Delta\tau \to 0$ extrapolation. For each size, this relative error is less than 1%.

	$L = 4$	$L = 6$	$L = 8$	$L = 10$
Trotter ($\times 10^{-3}$)	3.659	3.266	4.759	3.740
Finite-Size ($\times 10^{-3}$)	—	19.623	4.751	3.144
Statistical ($\times 10^{-3}$)	1.035	1.190	0.993	1.211

TABLE S2. Relative error of S_{cdw}/L^2, the CDW structure factor, caused by Trotter error, finite-size effects, and statistical error at $U = 3.5t, \mu = 0, T = t/4$ for each lattice size.

In Table S2, we compare the relative error from each source at the $U = 3.5t, \mu = 0, T = t/4$ point for the different lattice sizes. The Trotter error is given by the difference between the last data point ($t\Delta\tau = 1/24$) and the $t\Delta\tau \to 0$ extrapolated value. The finite-size error is

computed by the difference between the value for each lattice size and the value on the lattice one size smaller on the list. The statistical error is given by the standard deviation of the value as recorded by the DQMC algorithm. From these results, we see that these different sources of error are of a similar magnitude, with the statistical error generally being the smallest.

	$T = t/2$	$T = t/3$	$T = t/4$
Numerical Differentiation ($\times 10^{-3}$)	0.049	1.462	0.542
Finite-Size ($\times 10^{-3}$)	0.200	1.000	0.080
Statistical ($\times 10^{-3}$)	1.304	0.484	0.255

TABLE S3. Absolute error on χ, the difference susceptibility, caused by the numerical differentiation, finite-size effects, and statistical error at $U = 3.5t, \mu = 0, L = 10$ for each temperature.

Similarly, we calculate the absolute error from the numerical differentiation process (as explained in SM Sec. IV), finite-size effects and the statistical error for χ at $U = 3.5t$, $\mu = 0$, and $L = 10$. As before, the finite-size error is given by the difference between the $L = 10$ and $L = 8$ data points, and statistical error is given by the standard deviation of the observable as reported by our DQMC algorithm. These results are shown in Table S3. For the lower temperatures, the largest source of error is typically from the numerical differentiation.

VII. DIFFERENCE SUSCEPTIBILITY

There is no standard numerically accessible method to detect the formation of bound states in previous work on three-component fermions. The trion density $n^{(3)}$ is in part related to trion formation [7], however, the trion density can be non-zero even without bound trions, simply due to three particles occupying the same site. Additionally, even if a trion is centered at a site i, $n_i^{(3)}$ need not be equal to 1, because fluctuations (thermal or quantum when $t/U \neq \infty$) cause the trion to have some finite extent. Instead, we note that for large U/t the leading fluctuations of the trion are to adjacent dimers and singly-occupied sites, so that in a dilute gas of trions $n_d = n^{(2)} - n^{(1)}$ will vanish, in contrast to a gas or liquid of individual particles. The reason we take the derivative of n_d with respect to μ is because n_d can vanish for another reason – particle-hole symmetry – but χ will remain finite. With this motivation, the numerics indeed reveal a rather sharp feature in χ at low-temperature, consistent with the idea of a trion-singlon crossover.

Ref. [10] notes a method of detecting trion formation using the persistent current around a ring. This method seems promising, but it requires adding magnetic flux terms to our Hamiltonian. Along with increasing the number of DQMC runs needed, this term may also contribute to the sign problem.

In Fig. S6 we present the difference susceptibility along with the density of triply-occupied sites, $n^{(3)}$ and the derivatives of $n^{(1)}$ and $n^{(2)}$ with respect to μ/t. In the upper panel, it is clear that χ indicates a sharp crossover region that is not visible in $n^{(3)}$. The quantities $\frac{\partial\langle n^{(1)}\rangle}{\partial\mu}$ and $\frac{\partial\langle n^{(2)}\rangle}{\partial\mu}$ also display similar behavior to χ at half-filling. We also observe that in the more dilute regime, χ continues to quickly approach zero at large U/t, while $\frac{\partial\langle n^{(1)}\rangle}{\partial\mu}$, $\frac{\partial\langle n^{(2)}\rangle}{\partial\mu}$, and $n^{(3)}$ approach zero much more slowly. This evidence, along with the physical intuition for why $\chi \to 0$ as virtual dissociation becomes relevant gives a justification for using χ as our trion-formation indicator.

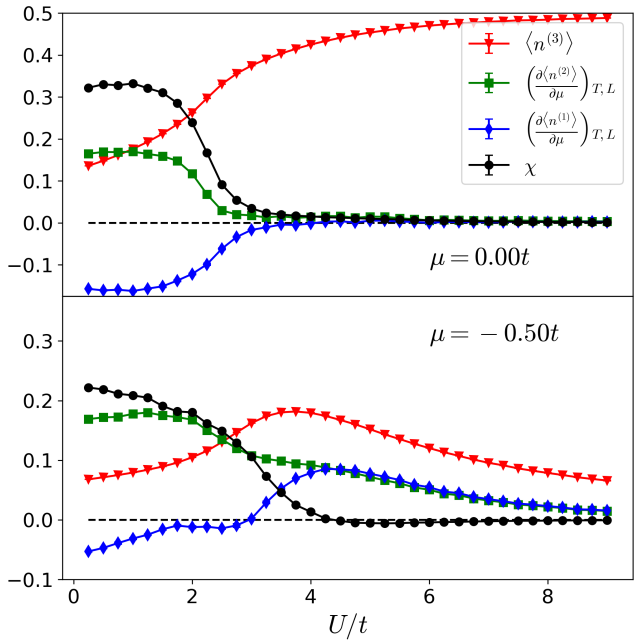

FIG. S6. The difference susceptibility, χ, fraction of triply-occupied sites, $n^{(3)}$ and derivatives of $n^{(1)}$ and $n^{(2)}$ with respect to μ as functions of U/t at two different μ/t values. We set $T = t/3$ and $L = 10$ for this data. Error bars are smaller than the data markers.

While the difference susceptibility indicates trion formation in this work, there are also limitations to our approach. In particular, since the difference susceptibility depends on reasoning about perturbing around specific eigenstates, it cannot detect the formation of trions in a thermal mixture with unbound fermions. Further development in detecting bound states using data available to DQMC calculations or experimental setups may be needed to better understand trion formation at higher temperatures.

VIII. ON-SITE DENSITY

The DQMC method works in the grand canonical ensemble, which means the total density, $\langle n\rangle = \frac{1}{L^2}\sum_{i,\sigma}\langle n_{i\sigma}\rangle$, changes with parameters in the Hamilto-

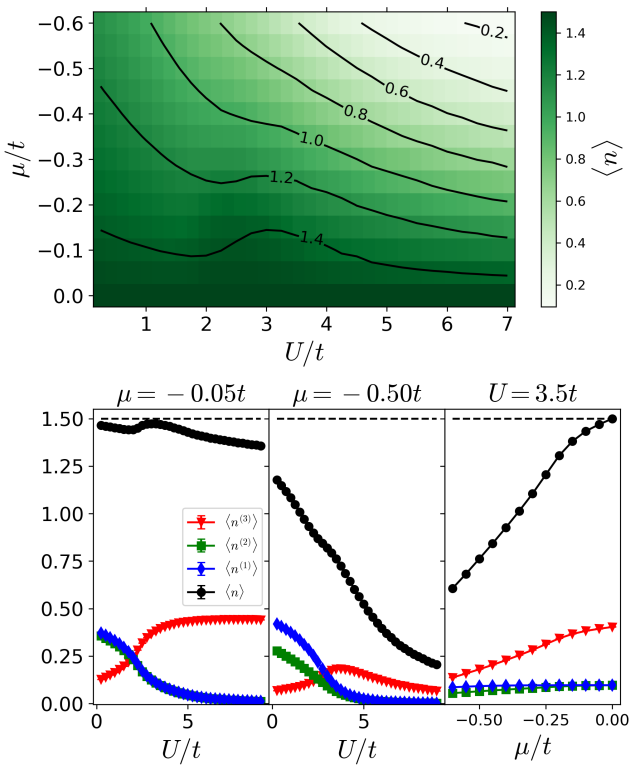

FIG. S7. The top plot shows the total density, $\langle n\rangle$, for $L = 10$ and $T = t/3$ along with contour lines to guide the eye. The lower plots shows $\langle n\rangle$ along with $\langle n^{(1)}\rangle$, $\langle n^{(2)}\rangle$, and $\langle n^{(3)}\rangle$ cuts at $\mu = -0.05t$, $\mu = -0.5t$, and $U/t = 3.5t$ again at $L = 10$ and $T = t/3$. Error bars are shown but often smaller than data points.

nian. In Fig. S7, we plot the total density at some representative data points. In the $T = t/3$ cut shown, the density ranges from $\langle n\rangle = 1.5$ (half-filling) to $\langle n\rangle \approx 0.1$ in the top right corner.

We have written our Hamiltonian in a form where $\mu/t = 0$ corresponds to $n = 3/2$ (half-filling). That is, when $\mu/t = 0$ the Hamiltonian $H = Q + V$ is invariant under the transformation

$$\begin{cases} c_{i\sigma} & \to (-1)^i c^\dagger_{i\sigma} \\ c^\dagger_{i\sigma} & \to (-1)^i c_{i\sigma}, \end{cases} \tag{S30}$$

where the site index i is even on one sublattice and odd on the other. This is the particle-hole symmetry of the SU(N) Fermi-Hubbard model, and persists for any value of N and for both the attractive and repulsive cases. If $\mu \neq 0$, this transformation flips the sign of μ, which means observables at a given μ/t are equal to their particle-hole transformed values at $-\mu/t$.

For the general SU(N) case, the transformation

$$\mu \to \mu + \frac{U(N-1)}{2} \tag{S31}$$

changes the on-site interaction into $-U\sum_{i,\sigma<\tau} n_{i\sigma}n_{i\tau}$, which is another common form for the interaction (especially for the SU(2) case) which makes the density-density nature of the interaction more apparent.

IX. THE MERMIN-WAGNER THEOREM AND SU(N) CDW ORDER

According to the Mermin-Wagner theorem [11], a continuous symmetry is not broken at finite temperature in one or two dimensions. This theorem prevents a finite-temperature CDW phase in the $N = 2$ attractive FHM, owing to a continuous generalization of particle-hole symmetry that relates CDW order to s-wave superconductivity, but does not prevent a phase transition at finite temperature for $N > 2$. Here, we will derive the continuous symmetry which prevents the finite-temperature CDW phase in the $N = 2$ case and show that it is reduced to a discrete symmetry for $N > 2$.

$N = 2$ case: First, we introduce the operator

$$\eta^- = \sum_{\mathbf{r}} e^{-i\mathbf{Q}\cdot\mathbf{r}} c_{\mathbf{r}\uparrow}c_{\mathbf{r}\downarrow} = \sum_{\mathbf{k}} c_{\mathbf{k}\uparrow}c_{\mathbf{Q}-\mathbf{k}\downarrow}, \tag{S32}$$

(where $\mathbf{Q} = (\pi,\pi)$), its Hermitian conjugate, $\eta^+ = (\eta^-)^\dagger$, and

$$\eta^z \equiv \frac{1}{2}[\eta^+,\eta^-] = \frac{1}{2}\left(\sum_{i,\sigma} n_{i\sigma} - L^2\right), \tag{S33}$$

where the σ index runs over $\{\uparrow,\downarrow\}$. After verifying the commutation relations

$$[\eta^z,\eta^\pm] = \pm\eta^\pm \tag{S34}$$

we see that

$$\eta^x = \frac{1}{2}\left(\eta^+ + \eta^-\right) \tag{S35}$$

$$\eta^y = \frac{i}{2}\left(\eta^- - \eta^+\right) \tag{S36}$$

along with η^z are the generators of an $\mathfrak{su}(2)$ algebra.

Furthermore, we can show that

$$[H,\eta^\pm] = \mp 2\mu\eta^\pm \tag{S37}$$

$$[H,\eta^z] = 0. \tag{S38}$$

Therefore, when $\mu = 0$ (half-filling), these operators all commute with H and there is an SU(2) symmetry of H generated by η^x,η^y,η^z. Note that the typical form of these commutators found in the literature can be recovered under the transformation in Eq. (S31).

The particle-hole symmetry can be expressed using these generators. In particular, $\exp(-i\pi\eta^y)$ is the transformation,

$$\begin{cases} c_{i\uparrow} & \to (-1)^i c^\dagger_{i\downarrow} \\ c_{i\downarrow} & \to (-1)^i c^\dagger_{i\uparrow} \\ c^\dagger_{i\uparrow} & \to (-1)^i c_{i\downarrow} \\ c^\dagger_{i\downarrow} & \to (-1)^i c_{i\uparrow} \end{cases}, \tag{S39}$$

which can be combined with a transformation which swaps ↑ and ↓ to recover the $N = 2$ particle-hole symmetry shown in Eq. (S30). So, since the particle-hole symmetry of the $N = 2$ Fermi-Hubbard model is an element of a continuous symmetry group, and since a CDW phase transition breaks particle-hole symmetry, the Mermin-Wagner theorem prohibits the CDW phase transition from occurring at finite temperature.

***N* > 2 case:** In this work, we have observed a finite-temperature CDW phase transition for $N = 3$, even though the $N = 3$ FHM still possesses a particle-hole symmetry. This is because, for $N > 2$, the particle-hole symmetry is not a member of a continuous symmetry group. To demonstrate why the above argument for a continuous SU(2) symmetry in the $N = 2$ case does not generalize for $N > 2$, we will first give more detail on why, for $N = 2$, $[V, \eta^+] = 0$, where $H = Q + V$ as defined in Eq. (S2).

Following an argument from Ref. [12], we notice that V is diagonal in the basis of position-indexed Fock states. So, for arbitrary Fock states $|n\rangle$ and $|n'\rangle$, the associated matrix element of the commutator can be written as

$$\begin{aligned}\langle n|[V,\eta^+]|n'\rangle &= \langle n|V\eta^+ - \eta^+V|n'\rangle \\ &= (\langle n|V|n\rangle - \langle n'|V|n'\rangle)\ \langle n|\eta^+|n'\rangle \\ &= C_{nn'}\langle n|\eta^+|n'\rangle \end{aligned} \tag{S40}$$

For some coefficient $C_{nn'}$ which depends on states $|n\rangle$ and $|n'\rangle$. It is clear that a matrix element of this commutator is non-zero only if the corresponding matrix element of η^+ is non-zero. This is only true when $|n\rangle = c^\dagger_{i\sigma}c^\dagger_{i\tau}|n'\rangle$ for some site i and $\sigma \neq \tau$. This means that, for $N = 2$, $\sigma \in \{\uparrow, \downarrow\}$,

$$\begin{aligned} C_{nn'} &= \langle n|V|n\rangle - \langle n'|V|n'\rangle \\ &= -\frac{U}{2}\left(\langle n|\left(\sum_\sigma n_{i\sigma} - \frac{N}{2}\right)^2|n\rangle \right. \\ &\quad \left. - \langle n'|\left(\sum_\sigma n_{i\sigma} - \frac{N}{2}\right)^2|n'\rangle\right), \\ &= -\frac{U}{2}\left((2-1)^2 - (0-1)^2\right) \\ &= 0, \end{aligned} \tag{S41}$$

which is independent of $|n\rangle, |n'\rangle$. However, if $N > 2$, $C_{nn'}$ can attain a non-zero value which depends on $|n\rangle, |n'\rangle$. In this case, η^+ does not commute with H at half-filling, which means $\eta^\pm$ and η^z no longer generate a continuous SU(2) symmetry. So, even though the Mermin-Wagner theorem states that a continuous symmetry cannot be spontaneously broken at finite temperature, a finite-temperature CDW phase transition is allowed for $N > 2$ but forbidden for $N = 2$.

[1] D. J. Scalapino and R. L. Sugar, Monte Carlo calculations of coupled boson-fermion systems. II, Phys. Rev. B **24**, 4295 (1981).

[2] E. Y. Loh, J. E. Gubernatis, R. T. Scalettar, S. R. White, D. J. Scalapino, and R. L. Sugar, Sign problem in the numerical simulation of many-electron systems, Phys. Rev. B **41**, 9301 (1990).

[3] M. Troyer and U.-J. Wiese, Computational complexity and fundamental limitations to fermionic quantum monte carlo simulations, Phys. Rev. Lett. **94**, 170201 (2005).

[4] R. Mondaini, S. Tarat, and R. T. Scalettar, Quantum critical points and the sign problem, Science **375**, 418 (2022).

[5] K. Binder, Finite size scaling analysis of Ising model block distribution functions, Z. Phys. B **43**, 119 (1981).

[6] R. K. Kaul, Spin nematics, valence-bond solids, and spin liquids in SO(N) quantum spin models on the triangular lattice, Phys. Rev. Lett. **115**, 157202 (2015).

[7] H. Xu, X. Li, Z. Zhou, X. Wang, L. Wang, C. Wu, and Y. Wang, Trion states and quantum criticality of attractive SU(3) Dirac fermions, Phys. Rev. Res. **5**, 023180 (2023).

[8] K. L. Lee, K. Bouadim, G. G. Batrouni, F. Hébert, R. T. Scalettar, C. Miniatura, and B. Grémaud, Attractive Hubbard model on a honeycomb lattice: Quantum monte carlo study, Phys. Rev. B **80**, 245118 (2009).

[9] D. A. Huse, Ground-state staggered magnetization of two-dimensional quantum Heisenberg antiferromagnets, Physical Review B **37**, 2380 (1988).

[10] W. J. Chetcuti, J. Polo, A. Osterloh, P. Castorina, and L. Amico, Probe for bound states of SU(3) fermions and colour deconfinement, Commun. Phys. **6**, 1 (2023).

[11] N. D. Mermin and H. Wagner, Absence of ferromagnetism or antiferromagnetism in one- or two-dimensional isotropic Heisenberg models, Phys. Rev. Lett. **17**, 1133 (1966).

[12] C. N. Yang, η pairing and off-diagonal long-range order in a Hubbard model, Phys. Rev. Lett. **63**, 2144 (1989).